LES – DFSD modelling of vented hydrogen explosions in a small-scale combustion chamber

M. Elshimy [a,*], S. Ibrahim [a] and W. Malalasekera [b]

[a] Department of Aeronautical and Automotive Engineering, Loughborough University, Loughborough, LE11 3TU, UK

[b] Wolfson School of Mechanical, Electrical and Manufacturing Engineering, Loughborough University, Loughborough, LE11 3TU, UK

Abstract

Accidental explosions are a plausible danger to the chemical process industries. In the event of a gas explosion, any obstacles placed within the path of the flame generate turbulence, which accelerates the transient flame and raises explosion overpressure, posing a safety hazard. This paper presents numerical studies using an in-house computational fluid dynamics (CFD) model for lean premixed hydrogen/air flame propagations with an equivalence ratio of 0.7. A laboratory-scale combustion chamber is used with repeated solid obstacles. The transient compressible large eddy simulation (LES) modelling technique combined with a dynamic flame surface density (DFSD) combustion model is used to carry out the numerical simulations in three-dimensional space. The study presented uses eight different baffle configurations with two solid obstructions, which have area blockage ratios of 0.24 and 0.5. The flame speed, maximum rate of pressure-rise as well as peak overpressure magnitude and timing are presented and discussed. Numerical results are validated against available published experimental data. It is concluded that, increasing the solid obstacle area blockage ratio and the number of consecutive baffles results in a raised maximum rate of pressure rise, higher peak explosion overpressure and faster flame propagation. Future model development would require more experimental data, probably in a more congested configuration.

Introduction

Hydrogen benefits from its high energy density and renewability when compared to alternative hydrocarbons (Møller et al., 2017). There are multiple renewable methods to harvest green energy, which consider the urban impact of the fuel extraction process (Tong et al., 2018). A fuel/air mixture prone to combustion can be generated as a result of a flammable gas such as hydrogen (H_2) being accidentally released into the atmosphere. If accidental ignition occurs from an external source, flame deflagration is likely to follow. This deflagration can result in high combustion overpressure, particularly in the presence of solid obstructions. In many situations, the danger is posed by the peak combustion overpressure rather than the high temperatures of the transient flame. Key parameters such as the timing and magnitude of peak overpressure are essential for consideration by design and safety engineers. As a result, there is increasing demand for adequate modelling techniques which can carry out such predictions to ensure the safety of process industries. Several factors can influence the overpressure magnitude and timing including obstacle area blockage ratio, obstruction separation distance, mixture strength and the type of fuel (Al-Harbi, 2013; Al-Harbi et al., 2014; Ibrahim et al.,

* Corresponding author.
E-mail address: m.a.a.a.elshimy@lboro.ac.uk

2009; Ibrahim and Masri, 2001; Masri et al., 2011; Na'inna et al., 2013). Some algebraic attempts have been made to predict explosion overpressure in specific conditions, however the drawback of these numerical approaches is that the generated turbulence is not taken into consideration (Bjerketvedt et al., 1997).

Computational Fluid Dynamics (CFD) has been introduced to the process industries relatively recently, with improvements in the technique resulting in it being a suitable alternative to experiments (Both et al., 2019; Diakow et al., 2018; Fiates et al., 2016; Middha, 2010; Middha et al., 2009; Mouilleau and Champassith, 2009). The most frequently used CFD techniques include the Reynolds-averaged Navier-Stokes (RANS) approach, direct numerical simulation (DNS) and large eddy simulations (LES) (Versteeg and Malalasekera, 2007). Than RANS approach has been successfully used to investigate the safety aspect of accidents and explosions for applicable structures (Catlin et al., 1995; Efthimiou et al., 2017; Huang et al., 2020; Popat et al., 1996). The RANS technique has also been applied to large scale applications, providing adequate results within the defined applications (Baraldi et al., 2017, 2010; Marangon et al., 2009; Vyazmina and Jallais, 2016). However, the drawback of using RANS is that the modelling technique is not the most accurate as a result of its averaging nature, meaning that some adjustment of model parameters is typically needed for satisfactory results. While DNS can provide highly accurate results, it usually requires considerable computational expense (Versteeg and Malalasekera, 2007). On the other hand, large eddy simulations explicitly resolve large scale flow and model the small-scale part of the flow. LES provides results to good degrees of accuracy without the required extensive computational resources vital to DNS. The LES technique has been accepted as an alternative modelling method which is more accurate than RANS as it is better in accounting for anisotropy and does not involve the same averaging characteristics of RANS. LES retains three dimensionality and can provide better predictions when compared to RANS for explosions in confined spaces, as obstacles can result in shear layers and wakes within recirculation zones in a highly turbulent environment. Applying the averaging approach to such studies would reduce the quality of numerical results. Several studies have used LES to provide predictions of explosions in various applications (Cheng et al., 2020; Cocks et al., 2015; Di Sarli et al., 2009; Ghani et al., 2015; Ibrahim et al., 2009; Jaravel et al., 2017; Li et al., 2016; R. Mercier et al., 2015; Molkov et al., 2006; Puggelli et al., 2021; Rochette et al., 2018; Schmitt et al., 2015; Veynante and Moureau, 2015; Volpiani et al., 2017; Wen et al., 2012). Examples of this is consist of investigating vented explosions, including hydrogen, in a laboratory scale combustion chamber (Abdel-Raheem et al., 2015; Di Sarli et al., 2009; S. R. Gubba et al., 2008; Sreenivasa Rao Gubba et al., 2008; Gubba et al., 2010, 2007; Li et al., 2018b, 2018a, 2018c, 2017; Makarov et al., 2007; Masri et al., 2006). For LES to be applicable to safety-related investigations, an appropriate sub-grid scale (SGS) combustion model, which can produce results for various flow conditions and mixtures, needs to be applied (Di Sarli et al., 2009; Makarov et al., 2007; Molkov et al., 2008). The Flame Surface Density (FSD) solves for a reaction progress variable and models the reaction rate as a function of the filter width. FSD models have been used for predictions of turbulent premixed combustion (Cant et al., 2004; Di Sarli et al., 2009; S. R. Gubba et al., 2008; Williamson et al., 2005). Previous research has

shown the importance of the FSD based SGS approach using LES (Boger et al., 1998; Hawkes and Cant, 2000; Ma et al., 2013). The Dynamic Flame Surface Density (DFSD) model expands on the FSD model by dynamically evaluating the SGS portion of the flame wrinkling (Wang et al., 2012). The DFSD model was initially applied for predicting an expanding turbulent flame and is expanded and applied to the present study. One of the primary advantages of this approach is its ability to adjust the model coefficient dynamically based on the resolved flame wrinkling. This is beneficial to the process industries, as an accidental explosion can have a flame change dynamically from initially laminar to fully turbulent as a result of repeated obstructions. Additionally, since the DFSD model is dynamic, it can outperform typical algebraic models without parameter tuning for applications of various scales.

It is imperative that LES is capable of reproducing all stages of an explosion generated flame for it to be applied to these numerous scales. An appropriate starting point is a lab-scale combustion chamber (Al-Harbi, 2013). This paper further validates the DFSD model (Gubba et al., 2007) using a lean hydrogen/air mixture applied with several baffle configurations and obstacles with two different area blockage ratios. Numerical results for the flame speed, rate of pressure rise, peak overpressure magnitude and timing will be validated against published experimental data. Numerical predictions are provided for flame speed where experimental equipment, and hence experimental data, was limited.

Experimental test case

Model validation is carried out using experimental data obtained from the lab-scale combustion chamber developed at the University of Sydney, Australia (Al-Harbi, 2013; Al-Harbi et al., 2014; Masri et al., 2011). The chamber schematic is shown in Fig. 1a. The chamber has a square cross-section and measures 50 x 50 x 250 mm (5:1 aspect ratio) and has a volume of 0.625 L. The chamber is equipped with three removable baffle plates positioned at 19 mm, 49 mm and 79 mm from the base of the chamber. As shown in Fig. 1b, each baffle is made of five 4 mm wide strips which are 3 mm in thickness, evenly spaced by 5 mm gaps. Each baffle provides an area blockage ratio of 0.4. A solid obstruction with a square cross section is placed 96 mm from the base of the chamber. Two square obstacles can be used with a small obstacle having a side length of 12 mm for an area blockage ratio of 0.24 or a large obstacle with a side length of 25 mm for an area blockage ratio of 0.5.

The mixture is introduced to the chamber via a non-return valve at atmospheric pressure. The lean hydrogen/air mixture (Φ=0.7) is then allowed to rest before ignition. The hinged flap at the top of the chamber is fully opened one second before ignition, and remains open for the length of the experiment, allowing for venting throughout the length of the explosion. Nd:YAG laser provides ignition by focusing an infrared output 2 mm above the base of the chamber. Ignition marks the start of the experiment.

Pressure readings are recorded with two Keller type PR21-SR piezo-electric pressure transducers at 25 kHz. One pressure transducer is placed in the base plate of the chamber and another is placed in the wall of the chamber 64 mm from the vent. Flame images are taken using high-speed laser-induced fluorescence from OH (LIF-OH) at 5 kHz.

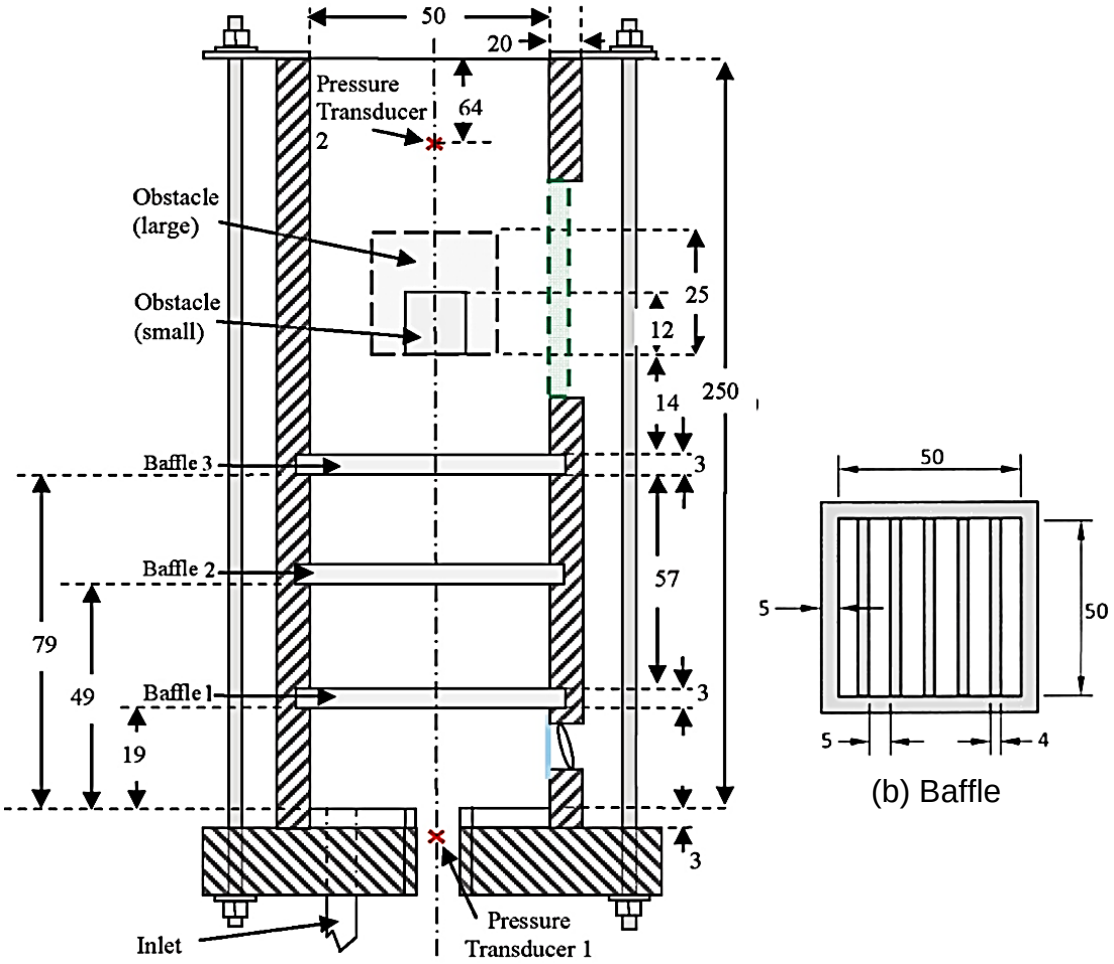

(a) Chamber

(b) Baffle

Fig. 1 – Combustion chamber schematic (a) and removable baffle (b) (all dimensions in mm, not to scale).

The current study uses 8 different baffle configurations which are shown in Fig. 2. Each configuration has a name based on the baffle arrangement and obstacle size. For example, configuration BBBL uses three consecutive baffles and a large square obstacle whereas configuration B0BS uses baffles 1 and baffle 3 combined with the small square obstacle. Experimental data used to validate numerical results in this paper is an average from minimum of 30 experiments.

Experimental limitations

Experiments using the lab-scale combustion chamber provided data for hydrogen at two equivalence ratios (Al-Harbi, 2013; Al-Harbi et al., 2014; Masri et al., 2011). However, due to hydrogen's high reactivity, the equivalence ratios were limited to 0.7 and 0.8. This is due to excessive overpressure at higher equivalence ratios which would exceed the 100 kPa (1000 mbar) limit of the pressure transducers (Masri et al., 2011). Combining an increased equivalence ratio with a solid obstacle of a higher ABR would further amplify explosion overpressures. LIF-OH images were captured for all configurations using the smaller obstacle. However, flame speed data is limited for configurations using the larger obstacle and is only available for configuration 0B0L. LIF-OH is able to capture the flame position and provide flame speed data due to the relatively low flame speed when this configuration is applied.

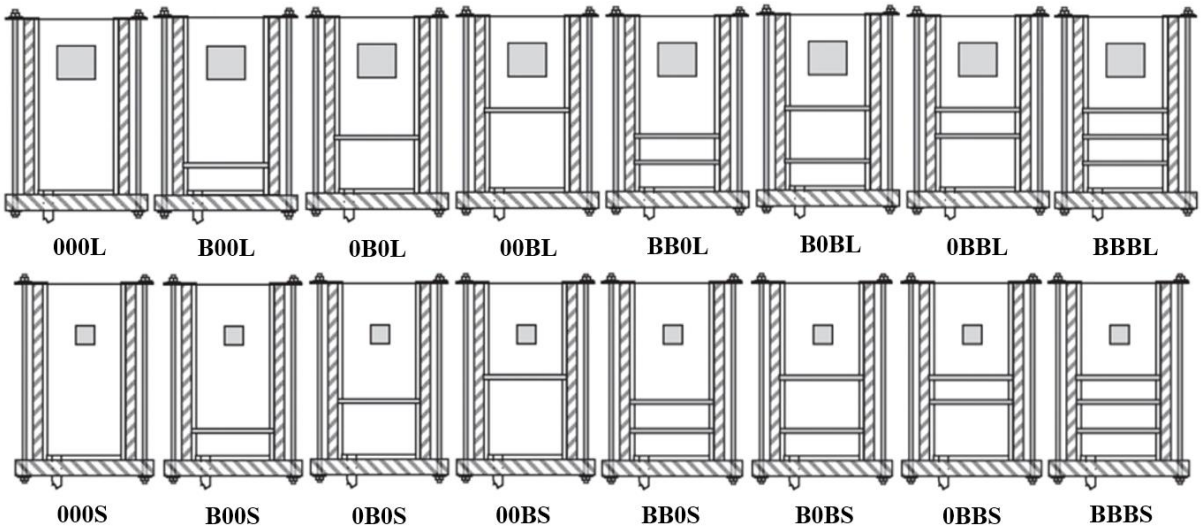

Fig. 2 – The 8 baffle configurations with combinations of the Large (L) or Small (S) obstacle.

Using configurations with additional baffles combined with the large obstacle result in higher transient flame speeds, which cannot be captured with the current flame imaging equipment. As a result, more advanced imaging equipment would be required to capture flame images and subsequently provide flame position and speed data for all configurations using the larger obstacle (ABR of 0.5) (Al-Harbi, 2013).

Numerical setup

Conservation equations for energy, mass and momentum govern numerical simulations for premixed combustion. The chemical state of the fuel/air mixture is identified by the Favre averaged reaction progress variable $\tilde{c}$. This is defined by $\tilde{c} = 1$ for a fully burned mixture and $\tilde{c} = 0$ for an unburned mixture. It can be challenging to model the reaction rate for turbulent premixed combustion as a result of complex interaction between turbulence levels, thermodynamic and chemical states. To simplify the system, a unity Lewis number is assumed, Zeldovich instability is neglected and a single step irreversible chemical reaction between reactants and products is applied. Further details on the numerical model are available elsewhere (Gubba et al., 2007).

The Favre averaged reaction progress variable $\tilde{c}$ is defined as:

$$\tilde{c} = 1 - \frac{m_f}{m_f^0} \tag{1}$$

where, m_f is the local fuel mass fraction and m_f^0 is the unburned fuel mass fraction in the mixture. The Favre-filtered transport equation for the reaction progress variable $\tilde{c}$ is given by the general form:

$$\frac{\partial \bar{\rho}\tilde{c}}{\partial t} + \frac{\partial}{\partial x_i}(\bar{\rho}\tilde{u}_i\tilde{c}) = -\frac{\partial}{\partial x_i}(\bar{\rho}\tilde{u}_i\tilde{c} - \bar{\rho}\tilde{u}_i\tilde{c}) + \overline{\frac{\partial}{\partial x_i}\left(\rho D \frac{\partial \tilde{c}}{\partial x_i}\right)} + \overline{\dot{\omega}_c} \tag{2}$$

Where $\overline{\dot{\omega}_c}$ is the filtered source term, which can be closed by the flame surface density concept as:

$$\overline{\dot{\omega}_c} = \rho_u S_L^0 \sum \tag{3}$$

where ρ_u is the fresh mixture density and S_L^0 is the un-strained laminar burning velocity. The sub-grid scale flame surface density $\sum$ is:

$$\sum = 4\sqrt{\frac{6}{\pi}}\Xi_\Delta \frac{\tilde{c}(1-\tilde{c})}{\Delta} \tag{4}$$

where Δ is the combustion filter width and Ξ_Δ is the sub-grid scale wrinkling factor. Previous research suggests that the combustion filter width Δ should be greater than the mesh size Δ_x enabling the filtered progress variable gradients to be well resolved when using an LES grid (Boger et al., 1998; Boger and Veynante, 2000; R Mercier et al., 2015; Wang et al., 2012). In this study the filter width used is 6 times the mesh size ($\Delta = 6\Delta_x$). Substituting equations (3) and (4) into the $\tilde{c}$ equation (2) gives (Boger, 2000; Boger et al., 1998):

$$\frac{\partial \bar{\rho}\tilde{c}}{\partial t} + \frac{\partial}{\partial x_i}(\bar{\rho}\tilde{u}_i\tilde{c}) = \frac{\partial}{\partial x_i}\left(\frac{\rho_u \Xi_\Delta S_L^0 \Delta}{16\sqrt{6/\pi}}\frac{\partial \tilde{c}}{\partial x_i}\right) + 4\rho_u S_L^0\sqrt{\frac{6}{\pi}}\Xi_\Delta\frac{\tilde{c}(1-\tilde{c})}{\Delta} \tag{5}$$

The modified diffusion term is included to control the thickness of the filtered flame and to apply the appropriate laminar burning velocity where the SGS turbulence is not present (Boger and Veynante, 2000; Ma et al., 2013; R Mercier et al., 2015). The sub-grid-scale flame wrinkling factor Ξ_Δ is described as a ratio of total and resolved flame surfaces locally, and accounts for the SGS flame surface lost through the filtering procedure. The SGS wrinkling factor is given by:

$$\Xi_\Delta = \left(\frac{\Delta}{\delta_c}\right)^\beta \tag{6}$$

Where δ_c is the inner cut-off scale as defined by the user and should be a multiple of the laminar flame thickness S_L^0 (R Mercier et al., 2015). The current study applies $\delta_c = 4S_L^0$. β is solved for dynamically by relating between the test-filtered and resolved flame front and is defined as:

$$\beta \approx \frac{\ln(\langle|\widehat{\nabla\tilde{c}}|\rangle/\langle\nabla\hat{\tilde{c}}\rangle)}{\ln\left(\sqrt{1+\left(\hat{\Delta}/\Delta\right)^2}\right)} \tag{7}$$

Where $\hat{\Delta}$ is the test filter width, the spatial averaging is defined by $\langle \dots \rangle$ and the test filtering is defined by $\widehat{\dots}$ and both are applied using an implemented Gaussian filter (Wang et al., 2011). The test-filter is set to $\hat{\Delta} = 1.1\Delta$ and the averaging-filter width is set to $\Delta_m = 3.0\hat{\Delta}$. The test filter width typically should be greater than the filtered flame thickness. The laminar burning velocity is set to 1.25 m/s and the thermal flame thickness is set at 0.12 mm for a hydrogen/air mixture with an equivalence ratio of 0.7 (Aung et al., 1997; Vermorel et al., 2017).

Computational setup

Numerical simulations for lean hydrogen explosions using LES are carried out using an in-house code called PUFFIN (Kirkpatrick, 2002). The finite volume method is applied on a Cartesian grid solving momentum, mass and scalar equations for compressible flows. The overall computational domain measures 325 x 325 x 500 mm in the x, y and z directions respectively.

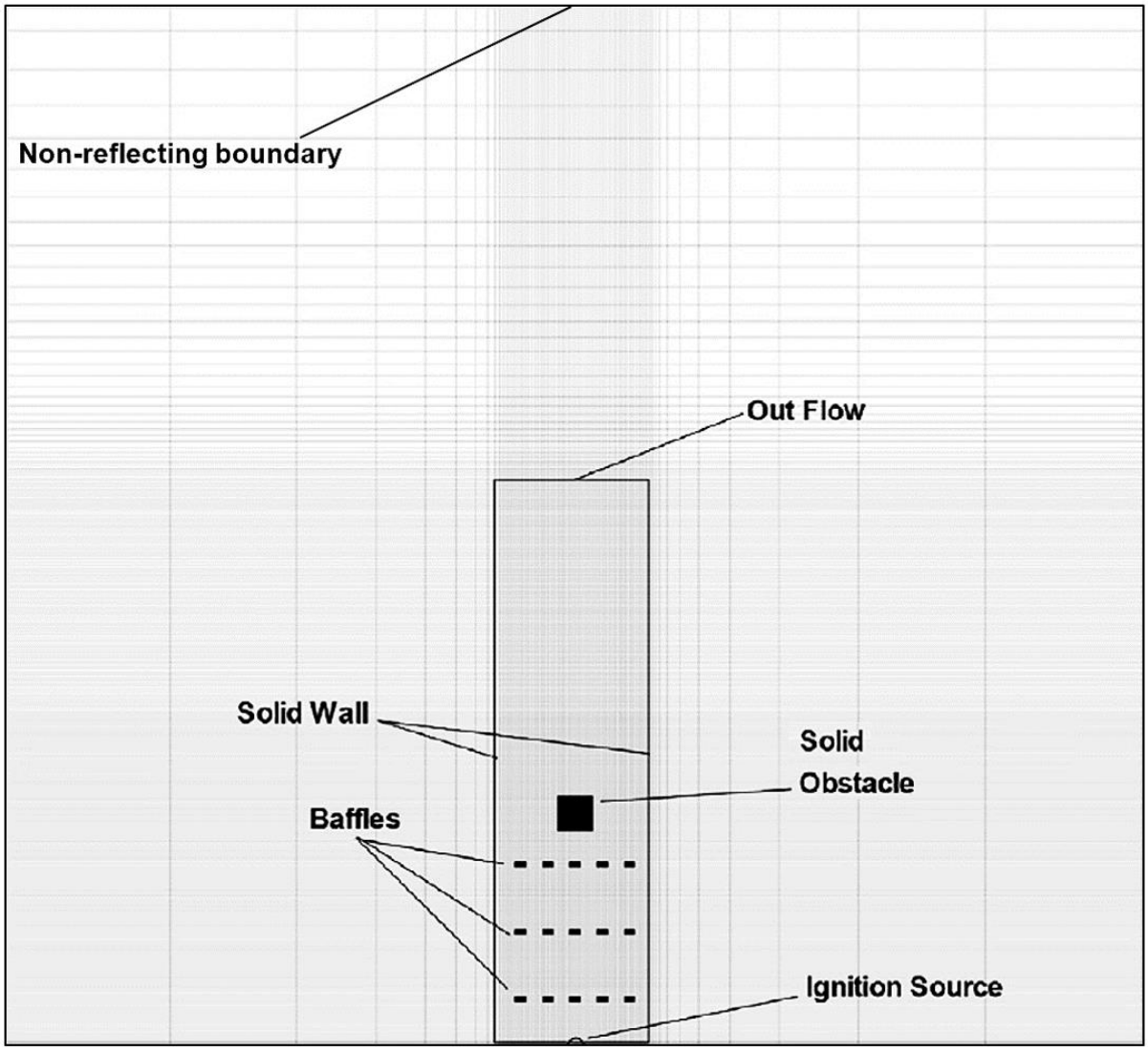

Fig. 3 – Computational domain showing combustion chamber, obstacles and grid resolution.

The computational domain is extended in the z direction, and non-reflecting far-field boundaries are applied to avoid pressure reflection effects. Within the computational domain, the combustion chamber measures 50 x 50 x 250 mm. Adiabatic and no-slip boundaries are applied to the solid walls of the chamber. The shear stress at the wall is solved for using the $1/7^{th}$ power law wall function developed by Werner and Wengle (Werner and Wengle, 1993). The dynamic Smagorinsky eddy viscosity model (Germano et al., 1991) is used for SGS turbulence modelling. The conservation equations for scalars use second-order central differencing scheme for diffusion terms. To avoid oscillation issues within the solution, the SHARP scheme is applied for advection terms of scalar equations (Leonard, 1979). Additional details

regarding the computational setup including the reaction mechanism, chemical model and boundary conditions can be found elsewhere (Kirkpatrick, 2002).
A computational grid resolution of 2.72 million cells (90 x 90 x 336) is applied following an extensive grid sensitivity study. Grid refinement is consistent for all baffle configurations and both solid obstacles. Increased grid resolution is applied to regions of increased flame-obstacle interaction. The grid refinement ensures that the filtered flame thickness is smaller than the spaces between the baffle plate strips. The grid refinement, chamber walls and obstructions are shown in Fig. 3. Ignition is initiated by introducing a burned flame kernel, defining a number of cells to have a reaction progress variable of 0.5. The kernel is located at the bottom of the chamber, where ignition would be initiated, and is hemispherical in shape, with 4 mm radius.

Results and discussion

Numerical results show flame-obstacle interaction and overpressures produced as a result of lean hydrogen/air explosions. Numerical results for the generated overpressure histories, rate of pressure rise and flame speeds from LES – DFSD model are compared with available experimental data. The primary focus of this study is to investigate maximum overpressure magnitude and timing following ignition as well as the maximum rate of pressure rise for two ABRs of 0.24 and 0.5.

Transient flame interaction with solid obstacles

Figure 4 shows high-speed LIF-OH experimental images of the transient hydrogen flame for configuration BBBS. Figures 5 and 6 show predicted LES – DFSD images of the Favre averaged reaction progress variable ($\tilde{c}$) for configurations BBBS and BBBL respectively. As mentioned earlier, imaging equipment was limited, and experimental images were not available for configuration BBBL with a lean hydrogen/air mixture. Regardless, a brief analysis is provided based on the numerical predictions provided. Time stamps at the top of each image provide the time since ignition, which marks the start of the experiment.

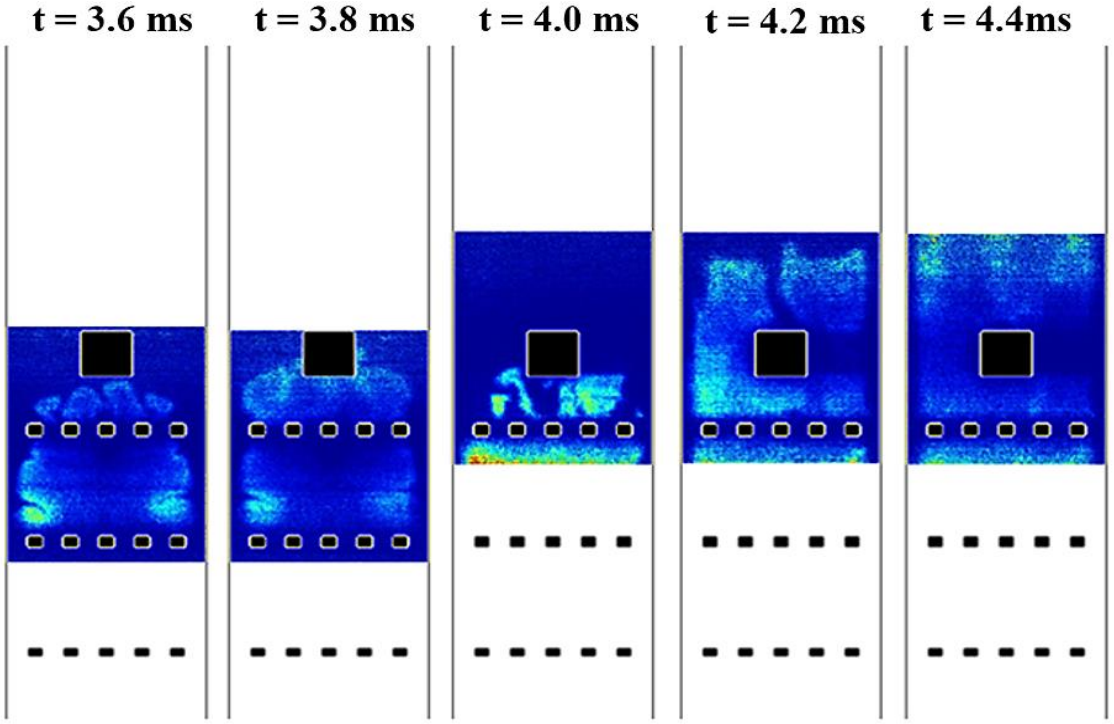

Fig. 4 – High-speed LIF-OH images of lean hydrogen/air flames using configuration BBBS (Al-Harbi, 2013).

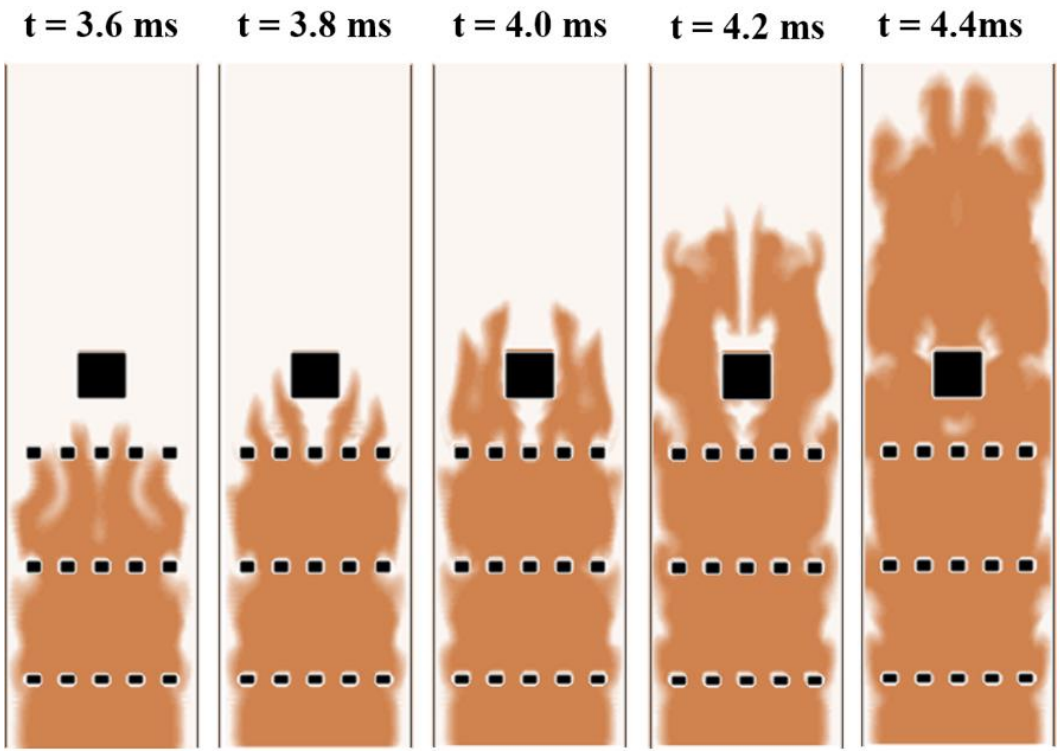

Fig. 5 – LES – DFSD results for the reaction progress variable for lean hydrogen/air flames using configuration BBBS.

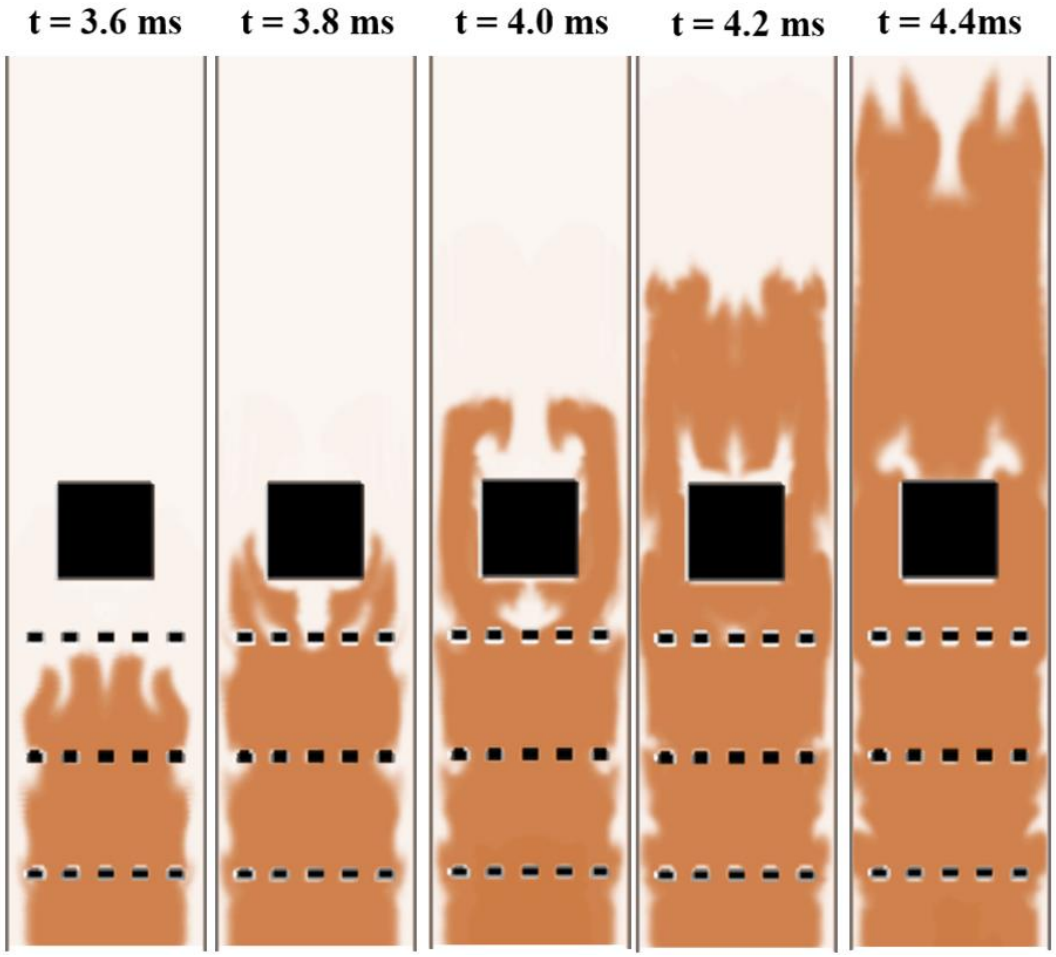

Fig. 6 – LES – DFSD predictions for the reaction progress variable for lean hydrogen/air flames using configuration BBBL.

The timeframes chosen in the images convey the flame as it jets through the final baffle, dividing into four separate channels. The flame then follows the path of least resistance on either side of the square obstruction. When the small square obstacle is used in configuration BBBS, there is a larger lateral area for the flame to spread and consume the unburnt mixture. The increased ABR of the solid obstacle affects the flame structure as a result of changes to the flow. When the flame reaches the square obstruction, there is also an initial slight reduction in the flame speed. As the flow travels past the obstacle it then recirculates behind the solid obstruction. As expected, a larger recirculating wake is created in Fig. 6 behind the larger obstacle when compared with Fig. 5. The large obstacle used in configuration BBBL has almost double the ABR, the flame is impeded by the increased blockage before proceeding to burn most of the fresh mixture on either side of the obstacle. A higher peak explosion overpressure and increased maximum rate of pressure rise is experienced as a result of this larger recirculating wake when using configuration BBBL is applied, as is conveyed by Figure 14. Similarly, the flame speeds then increase notably once the mixture in the wake is consumed. The flame subsequently consumes the remaining unburnt mixture within the chamber before travelling towards the vent at the top of the chamber. Good agreement in the flame structure as well as timing of the flame position and between Figures 3 and 4 confirms the capability of LES – DFSD to reproduce experimental data and provides confidence in future numerical predictions of the flame structure, such as those shown in Fig. 6.

Explosion characteristics: Overpressure

Overpressure-time histories are shown in Figures 7 through 14 for all possible configurations using 1, 2 and 3 baffles in every arrangement. In the figures, B1 refers to the first baffle, B2 refers to the second baffle and B3 identifies the third baffle. S denotes the small square obstacle whereas L represents the large square obstacle. Configurations 000L and 000S are also shown in Figure 7 and result in the lowest explosion overpressure. Since quasi-laminar combustion results in minimal explosion overpressure, it is not a major concern. The in-house code has subsequently been optimised for modelling fully turbulent combustion. As a result, numerical results offer a somewhat reduced accuracy for baffle arrangements with reduced turbulence. Configurations which have a large separation distance such as B00L or B00S also have relatively lower explosion overpressures due to a reduced turbulence intensity.

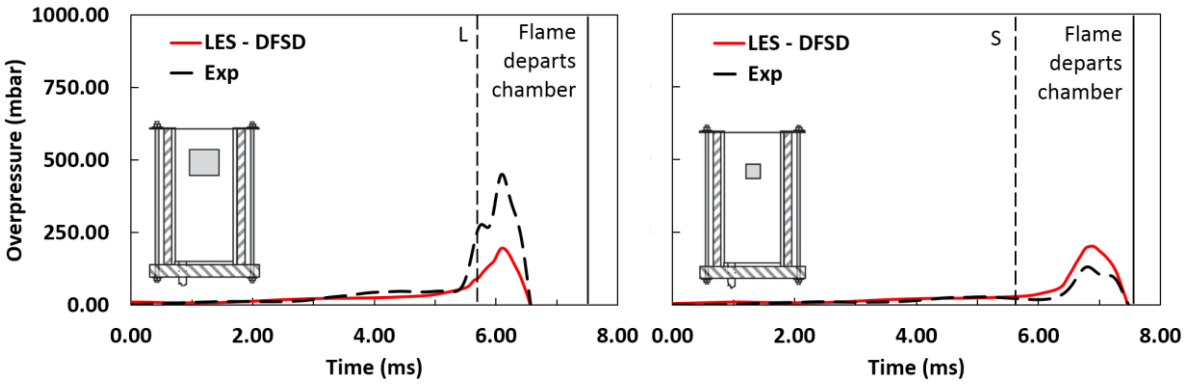

Fig. 7 – Overpressure-time traces for configuration 000L (left) and 000S (right).

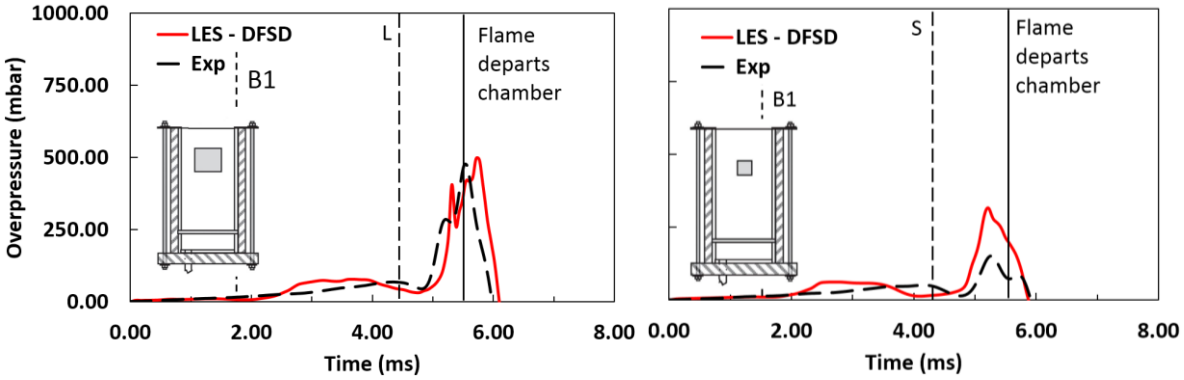

Fig. 8 – Overpressure-time traces for configuration B00L (left) and B00S (right).

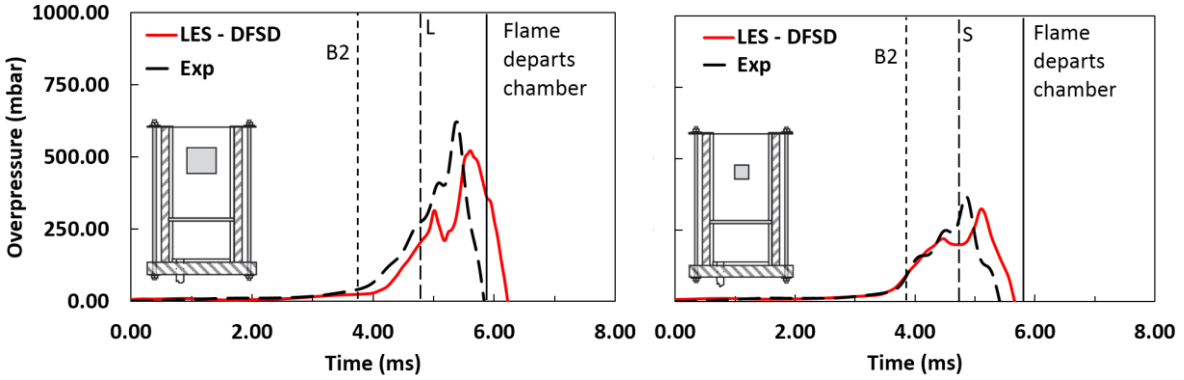

Fig. 9 – Overpressure-time traces for configuration 0B0L (left) and 0B0S (right).

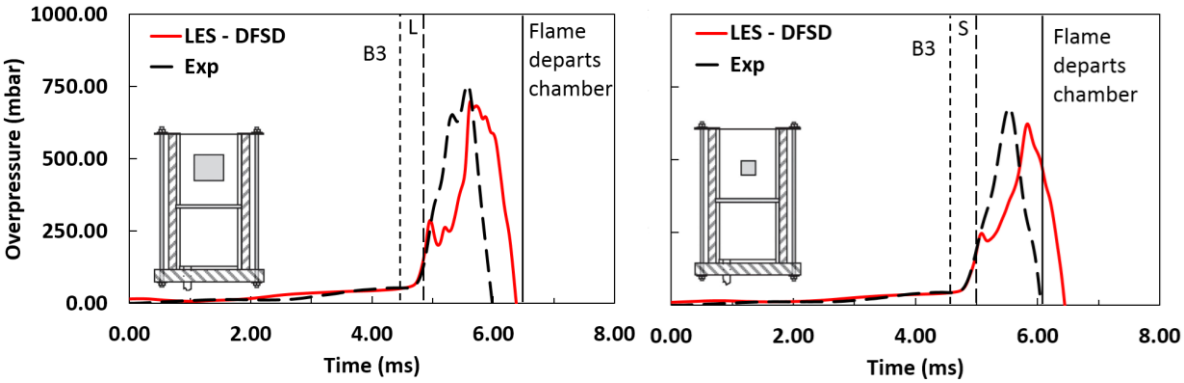

Fig. 10 – Overpressure-time traces for configuration 00BL (left) and 00BS (right).

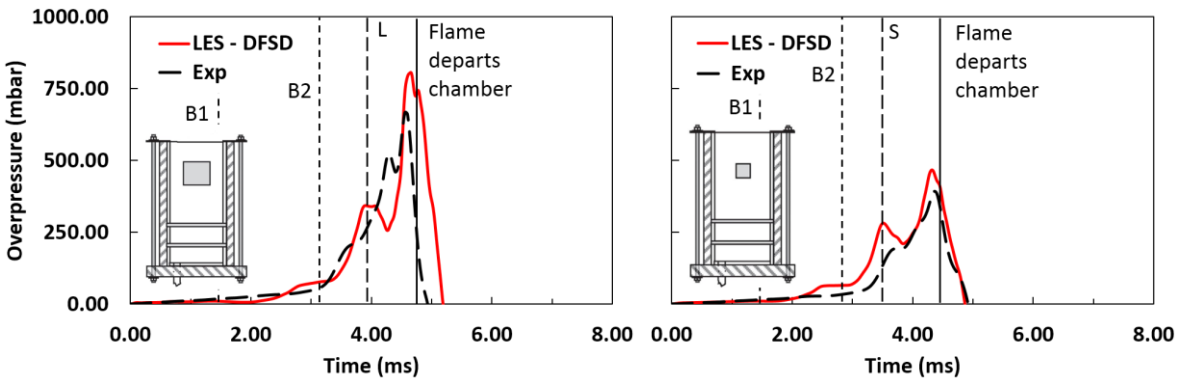

Fig. 11 – Overpressure-time traces for configuration BB0L (left) and BB0S (right).

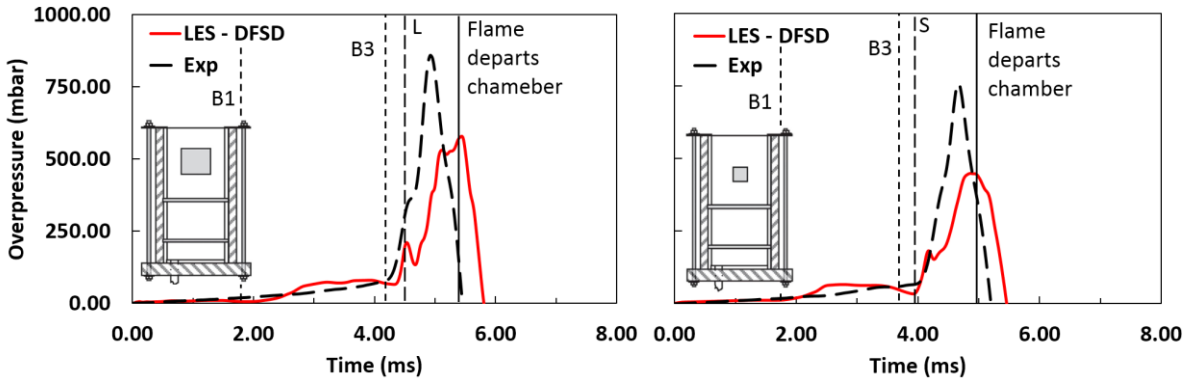

Fig. 12 – Overpressure-time traces for configuration B0BL (left) and B0BS (right).

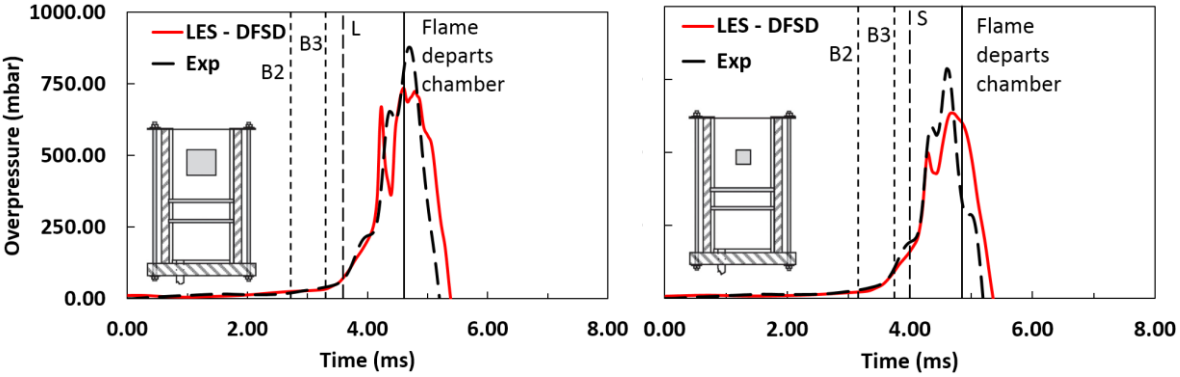

Fig. 13 – Overpressure-time traces for configuration 0BBL (left) and 0BBS (right).

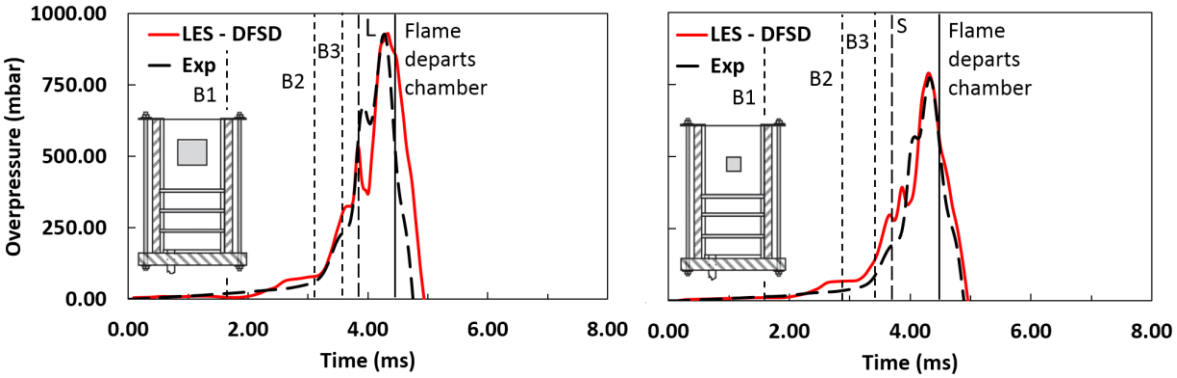

Fig. 14 – Overpressure-time traces for configuration BBBL (left) and BBBS (right).

Baffle configuration

Despite the lack of turbulence generated by a single baffle for configuration B00L, the peak combustion overpressure magnitude obtained experimentally of 475.37 mbar is well reproduced numerically at 499.26 mbar. Decreasing the obstacle separation distance raises the maximum explosion overpressure to 522.45 mbar for configuration 0B0L. The maximum rate of pressure rise for configuration 0B0L is 1.76×10^6 mbar/s which is as also well reproduced when compared to 1.84×10^6 mbar/s obtained experimentally. Configurations 00BL and 00BS have a minimum obstacle separation distance and hence produce the highest combustion overpressure for a single baffle configuration. A peak overpressure of 699.74 mbar is produced by configuration 00BL, whereas 623.83 mbar is obtained from configuration 00BS.

Placing an additional baffle raises the peak combustion overpressure and the maximum rate of pressure rise. For example, configuration 0B0S produced 324.30 mbar of peak combustion overpressure, which increases to 466.72 mbar when the baffle closest to the base of the chamber is added in configuration BB0S. Numerical results for configurations B0BL and B0BS in Figure 11 may not best represent experimental data, although the pressure rise and decay is well replicated. The maximum rate of pressure rise obtained numerically for configuration B0BL of 2.02×10^6 mbar/s accurately reflects the experimental 1.97×10^6 mbar/s.

Using three consecutive baffles results in the highest peak explosion overpressure. Additionally, since fully turbulent combustion is maintained, the pressure-histories using both the small and large obstacle represent the experimental data to a high degree of accuracy as shown in Figure 13. Configuration BBBL produces a peak explosion overpressure of 931.16 mbar and configuration BBBS produces 789.75 mbar.

Area blockage ratio

Increasing the square obstacle ABR results in an increased maximum explosion overpressure and a higher maximum rate of pressure rise across all baffle configurations. For example, the peak combustion overpressure for configuration B00S is 316.79 mbar, increases to 499.26 mbar for configuration B00L. The same trend is observed when looking at Figure 13, as configuration 0BBS produces 636.77 mbar whereas configuration 0BBL peaks at 735.95 mbar of overpressure. In Figure 14, configuration BBBL produces a maximum rate of pressure rise of 3.50×10^6 mbar/s while configuration BBBS has a peak rate of pressure rise of 3.00×10^6 mbar/s.

Explosion characteristics: flame speed

The flame position with respect to time is recorded experimentally by tracking the propagating flame front using high-speed LIF-OH images. Flame speed data is then subsequently obtained. As mentioned earlier, flame speed data is available for all configurations using a square obstacle with an ABR of 0.24. On the other hand, flame speed data is only available for configuration 0B0L when using an ABR of 0.5. Regardless, numerical predictions are provided below for the flame speed where experimental data is limited.

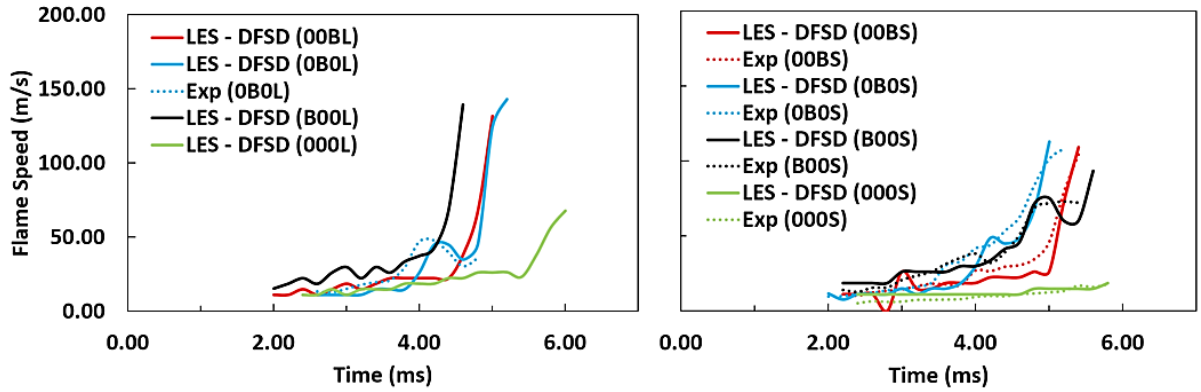

Fig.15 – Speed-time traces for configurations with up to one baffle with solid obstacle ABR 0.5 (left) and 0.24 (right).

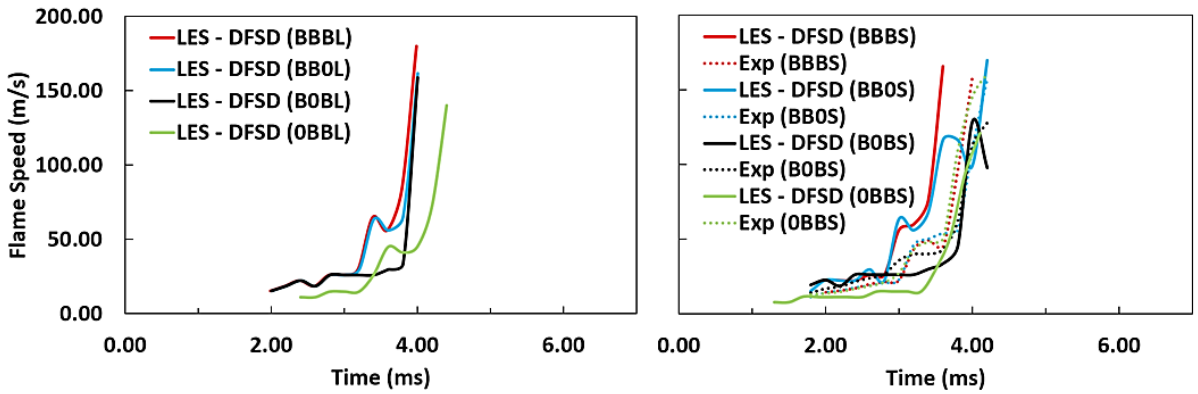

Fig. 16 – Speed-time traces for configurations with two or three baffles with solid obstacle ABR 0.5 (left) and 0.24 (right).

When comparing the flame speeds in Figures 15 and 16, it is clear to see that increasing the number of baffles progresively increases the transient flame speed. The maximum speed is also generally reached within a reduced timeframe. For example, configuration 000S reaches a maximum speed of 17.91 m/s at 5.80 ms. Configuration 00BS reaches a peak speed of 109.18 m/s at 5.40 ms. An additional baffle using configuration B0BS results in a raised maximum speed of 128.93 m/s at 4.00 ms. As expected, the highest speed for an ABR of 0.24 is attained by configuration BBBS at 165.71 m/s at 4.00 ms. Increasing the ABR of the square obstacle to 0.5 also raises the maximum flame speed as configuration 0B0L reaches 143.06 m/s at 5.20 ms whereas configuration 0B0S peaks at 108.46 m/s at the same time of 5.20 ms. The same trend is observed for results predicting flame speed across all additional configurations using the larger ABR when compared with the smaller ABR.

Conclusions

This paper presents an investigation of large eddy simulations (LES) with the dynamic flame surface density model (DFSD) numerically studying lean hydrogen explosions within a lab-scale explosion chamber. Eight different flow configurations are used with up to three solid baffles in all available combinations. The configurations are combined with a small obstacle (ABR of 0.24) and a large obstacle (ABR of 0.5). The LES – DFSD predictions are made where published experimental data is available. The following conclusions are made from the current study:

- The hydrogen flame is initially quasi-laminar before interaction with turbulence inducing baffles. Subsequently, successive baffles increase turbulence intensity and result in a fully turbulent flame.
- The numerical model is capable of reproducing the hydrogen flame structure as captured in experimental images.
- A decreased obstacle separation distance and an increased square obstruction ABR results in higher maximum overpressures and greater rates of pressure rise.
- Increasing the ABR and the number of baffles in the chamber results in higher flame speeds.

- Increased transient flame speeds are linked with a higher rate of pressure rise and greater peak explosion overpressure magnitudes.
- The LES – DFSD co-simulation model is capable of reproducing experimental data with high degrees of accuracy.
- More experimental measurements on hydrogen explosion with different mixture strength and/or homogeneity would be needed for further model developments.

Nomenclature

Δ	(mm)	LES combustion filter width
Δ_x	(mm)	Smallest computational cell width in the x direction
δ_c		Inner cut-off scale
$\tilde{c}$		Reaction progress variable
m_f		Local fuel mass fraction
m_f^0		Unburned fuel mass fraction
ρ	(kg/m^3)	Density
ρ_u	(kg/m^3)	Unburned mixture density
x_i		Direction in cartesian coordinate
$\overline{\dot{\omega}_c}$		Filtered source term
S_L^0	(m/s)	Un-strained laminar burning velocity
Ξ_Δ		Sub-grid scale wrinkling factor
$\langle \dots \rangle$		Volume averaging
$\widehat{\dots}$		Test filtering operation
D		Molecular diffusion coefficient
t	(s)	Time
ABR		Area blockage ratio
B1		First baffle plate
B2		Second baffle plate
B3		Third baffle plate
CFD		Computational fluid dynamics
FSD		Flame surface density
DFSD		Dynamic flame surface density
L		Large square obstacle
LES		Large eddy simulation
LIF-OH		Laser-induced fluorescence of OH
RANS		Reynolds-averaged Navier-Stokes
S		Small square obstacle
SGS		Sub-grid scale

R E F E R E N C E S

Abdel-Raheem, M.A., Ibrahim, S.S., Malalasekera, W., Masri, A.R., 2015. Large

eddy simulation of hydrogen-air premixed flames in a small scale combustion chamber. Int. J. Hydrogen Energy 40, 3098–3109. https://doi.org/10.1016/j.ijhydene.2014.12.042

Al-Harbi, A.A., 2013. Turbulent premixed flames propagating past repeated obstacles. Ph.D. Thesis. The Univeristy of Sydney.

Al-Harbi, A.A., Masri, A.R., Ibrahim, S.S., 2014. Turbulent premixed flames of CNG , LPG , and H2 propagating past repeated obstacles. Exp. Therm. Fluid Sci. 56, 2–8. https://doi.org/10.1016/j.expthermflusci.2013.11.012

Aung, K.T., Hassan, M.I., Faeth, G.M., 1997. Flame stretch interactions of laminar premixed hydrogen/air flames at normal temperature and pressure. Combust. Flame 109, 1–24.

Baraldi, D., Kotchourko, A., Lelyakin, A., Yanez, J., Gavrikov, A., Efimenko, A., Verbecke, F., Makarov, D., Molkov, V., Teodorczyk, A., 2010. An inter-comparison exercise on CFD model capabilities to simulate hydrogen deflagrations with pressure relief vents. Int. J. Hydrogen Energy 35, 12381–12390. https://doi.org/10.1016/j.ijhydene.2010.08.106

Baraldi, D., Melideo, D., Kotchourko, A., Ren, K., Yanez, J., Jedicke, O., Giannissi, S.G., Tolias, I.C., Venetsanos, A.G., Keenan, J., Makarov, D., Molkov, V., Slater, S., Verbecke, F., Duclos, A., 2017. Development of a model evaluation protocol for CFD analysis of hydrogen safety issues the SUSANA project. Int. J. Hydrogen Energy 42, 7633–7643. https://doi.org/10.1016/j.ijhydene.2016.05.212

Bjerketvedt, D., Bakke, J.R., Wingerden, K. Van, 1997. Gas explosion handbook. J. Hazard. Mater. 52, 1–150.

Boger, M., 2000. Modélisation de sous-maille pour la simulation aux grandes échelles de la combustion turbulente prémélangée. Ph.D. thesis. Ecole Centrale Paris.

Boger, M., Veynante, D., 2000. Large eddy simulations of a turbulent premixed v-shape flame, in: Eighth European Turbulence Conference. Dopazo, C, Barcelona, pp. 448–452. https://doi.org/http://dx.doi.org/10.1016/0142-727X(90)90030-F

Boger, M., Veynante, D., Boughanem, H., Trouve, A., 1998. Direct numerical simulation analysis of flame surface density concept for large eddy simulation of turbulent premixed combustion, in: Twenty-Seventh Symposium (International) on Combustion/The Combustion Institute. pp. 917–925.

Both, A.-L., Atanga, G., Hisken, H., 2019. CFD modelling of gas explosions: Optimising sub-grid model parameters. J. Loss Prev. Process Ind. 60, 159–173. https://doi.org/10.1016/j.jlp.2019.04.008

Cant, R.S., Dawes, W.N., Savill, A.M., 2004. ADVANCED CFD AND MODELING OF ACCIDENTAL EXPLOSIONS. Annu. Rev. Fluid Mech. 36, 97–119. https://doi.org/10.1146/annurev.fluid.36.050802.121948

Catlin, C.A., Fairweather, M., Ibrahim, S.S., 1995. Predictions of turbulent, premixed flame propagation in explosion tubes. Combust. Flame 102, 115–128.

Cheng, F., Chang, Z., Luo, Z., Liu, C., Wang, T., He, C., 2020. Large eddy simulation

and experimental study of the effect of wire mesh on flame behaviours of methane/air explosions in a semi-confined pipe. J. Loss Prev. Process Ind. 68, 104258. https://doi.org/10.1016/j.jlp.2020.104258

Cocks, P.A.T., Soteriou, M.C., Sankaran, V., 2015. Impact of numerics on the predictive capabilities of reacting flow LES. Combust. Flame 162, 3394–3411. https://doi.org/10.1016/j.combustflame.2015.04.016

Di Sarli, V., Di Benedetto, A., Russo, G., 2009. Using large eddy simulation for understanding vented gas explosions in the presence of obstacles. J. Hazard. Mater. J. 169, 435–442. https://doi.org/10.1016/j.jhazmat.2009.03.115

Diakow, P.A., Thomas, J.K., Vivanco, E., 2018. Comparison of large-scale vented deflagration tests to CFD simulations for partially congested enclosures. J. Loss Prev. Process Ind. 56, 147–154. https://doi.org/10.1016/j.jlp.2018.07.012

Efthimiou, G.C., Andronopoulos, S., Tavares, R., Bartzis, J.G., 2017. CFD-RANS prediction of the dispersion of a hazardous airborne material released during a real accident in an industrial environment. J. Loss Prev. Process Ind. 46, 23–36. https://doi.org/10.1016/j.jlp.2017.01.015

Fiates, J., Santos, R.R.C., Neto, F.F., Francesconi, A.Z., Simoes, V., Vianna, S.S.V., 2016. An alternative CFD tool for gas dispersion modelling of heavy gas. J. Loss Prev. Process Ind. 44, 583–593. https://doi.org/10.1016/j.jlp.2016.08.002

Germano, M., Piomelli, U., Moin, P., Cabot, W.H., 1991. A dynamic subgrid-scale eddy viscosity model. Phys. Fluids A 3, 1760–1765. https://doi.org/10.1063/1.857955

Ghani, A., Poinsot, T., Gicquel, L., Staffelbach, G., 2015. LES of longitudinal and transverse self-excited combustion instabilities in a bluff-body stabilized turbulent premixed flame. Combust. Flame 162, 4075–4083. https://doi.org/10.1016/j.combustflame.2015.08.024

Gubba, S.R., Ibrahim, S.S., Malalasekera, W., 2010. A parametric study on large eddy simulations of turbulent premixed flames, in: Proceedings of the Eighth Asia Pacific Conference on Combustion.

Gubba, S. R., Ibrahim, S.S., Malalasekera, W., Masri, A.R., 2008. LES modeling of premixed deflagrating flames in a small-scale vented explosion chamber with a series of solid obstructions. Combust. Sci. Technol. 180, 1936–1955. https://doi.org/10.1080/00102200802261852

Gubba, S.R., Ibrahim, S.S., Malalasekera, W., Masri, A.R., 2007. LES modelling of propagating turbulent premixed flames using a dynamic flame surface density model, in: 2nd ECCOMAS Thematic Conference on Computational Combustio.

Gubba, Sreenivasa Rao, Ibrahim, S.S., Malalasekera, W.M.G., 2008. A dynamic SGS model for LES of turbulent premixed flames, in: International Symposium on Advances in Computational Heat Transfer. https://doi.org/10.1615/ichmt.2008.cht.840

Hawkes, E.R., Cant, R.S., 2000. A flame surface density approach to large-eddy simulation of premixed turbulent combustion, in: Proceedings of the Combustion Institute. pp. 51–58.

Huang, C., Lipatnikov, A.N., Nessvi, K., 2020. Unsteady 3-D RANS simulations of dust explosion in a fan stirred explosion vessel using an open source code. J. Loss Prev. Process Ind. 67, 104237. https://doi.org/10.1016/j.jlp.2020.104237

Ibrahim, S.S., Gubba, S.R., Masri, A.R., Malalasekera, W., 2009. Calculations of explosion deflagrating flames using a dynamic flame surface density model. J. Loss Prev. Process Ind. 22, 258–264. https://doi.org/10.1016/j.jlp.2008.05.006

Ibrahim, S.S., Masri, A.R., 2001. The effects of obstructions on overpressure resulting from premixed flame deflagration. J. Loss Prev. Process Ind. 14, 213–221. https://doi.org/10.1016/S0950-4230(00)00024-3

Jaravel, T., Riber, E., Cuenot, B., Bulat, G., 2017. Large Eddy Simulation of an industrial gas turbine combustor using reduced chemistry with accurate pollutant prediction. Proc. Combust. Inst. 36, 3817–3825. https://doi.org/10.1016/j.proci.2016.07.027

Kirkpatrick, M.P., 2002. A large eddy simulation code for industrial and environmental flows. The University of Sydney.

Leonard, B.P., 1979. A stable and accurate convective modelling procedure based on quadratic upstream interpolation. Comput. Methods Appl. Mech. Eng. 19, 59–98.

Li, H.-G., Khare, P., Sung, H.-G., Yang, V., 2016. A Large-Eddy-Simulation Study of Combustion Dynamics of Bluff-Body Stabilized Flames. Combust. Sci. Technol. 188, 924–952. https://doi.org/10.1080/00102202.2015.1136296

Li, R., Malalasekera, W., Ibrahim, S., 2018a. LES-DFSD modelling of turbulent premixed flames past repeated obstacles, in: Proceedings of the 3rd World Congress on Momentum, Heat and Mass Transfer. pp. 1–8. https://doi.org/10.11159/csp18.108

Li, R., Malalasekera, W., Ibrahim, S., 2018b. Numerical study of vented hydrogen explosions in a small scale obstructed chamber. Int. J. Hydrogen Energy 43, 16667–16683. https://doi.org/10.1016/j.ijhydene.2018.07.078

Li, R., Malalasekera, W., Ibrahim, S.S., 2017. Numerical investigation of early flame propagation in vented explosions. Tenth Mediterr. Combust. Symp.

Li, R., Malalasekera, W., Ibrahim, S.S., Liu, B., 2018c. On the mechanism of pressure rise in vented explosions: A numerical study. IChemE 117, 551–564. https://doi.org/10.1016/j.psep.2018.05.026

Ma, T., Stein, O.T., Chakraborty, N., Kempf, A.M., 2013. A posteriori testing of algebraic flame surface density models for LES. Combust. Theory Model. 17, 431–482. https://doi.org/10.1080/13647830.2013.779388

Makarov, D., Molkov, V., Gostintsev, Y.U., 2007. Comparison between RNG and fractal combustion models for LES of unconfined explosions. Combust. Sci. Technol. 179, 401–416. https://doi.org/10.1080/00102200600835626

Marangon, A., Schiavetti, M., Carcassi, M., Pittiglio, P., Bragatto, P., Castellano, A., 2009. Turbulent hydrogen deflagration induced by ostacles in real confined environment. Int. J. Hydrogen Energy 34, 4669–4674. https://doi.org/10.1016/j.ijhydene.2008.07.053

Masri, A.R., Al-Harbi, A.A., Meares, S., Ibrahim, S.S., 2011. A comparative study of turbulent premixed flames propagating past repeated obstacles. Ind. Eng. Chem. Res. 51, 7690–7703. https://doi.org/10.1021/ie201928g

Masri, A.R., Ibrahim, S.S., Cadwallader, B.J., 2006. Measurements and large eddy simulation of propagating premixed flames. Exp. Therm. Fluid Sci. 30, 687–702. https://doi.org/10.1016/j.expthermflusci.2006.01.008

Mercier, R, Moureau, V., Veynante, D., Fiorina, B., 2015. LES of turbulent combustion:on the consistency between flame and flow filter scales, in: Combust. Inst. 35. pp. 1359–1366. https://doi.org/http://dx.doi.org/10.1016/j.proci.2014.05.149

Mercier, R., Schmitt, T., Veynante, D., Fiorina, B., 2015. The influence of combustion SGS submodels on the resolved flame propagation. Application to the LES of the Cambridge stratified flames. Proc. Combust. Inst. 35, 1259–1267. https://doi.org/10.1016/j.proci.2014.06.068

Middha, P., 2010. Development, use, and validation of the CFD tool FLACS for hydrogen safety studies. Ph.D. thesis. University of Bergen.

Middha, P., Hansen, O.R., Storvik, I.E., 2009. Validation of CFD-model for hydrogen dispersion. J. Loss Prev. Process Ind. 22, 1034–1038. https://doi.org/10.1016/j.jlp.2009.07.020

Molkov, V., Makarov, D., Puttock, J., 2006. The nature and large eddy simulation of coherent deflagrations in a vented enclosure-atmosphere system. J. Loss Prev. Process Ind. 19, 121–129. https://doi.org/10.1016/j.jlp.2005.05.006

Molkov, V., Verbecke, F., Makarov, D., 2008. LES of hydrogen-air deflagrations in a 78.5-m tunnel. Combust. Sci. Technol. 180, 796–808. https://doi.org/10.1080/00102200801893994

Møller, K.T., Jensen, T.R., Akiba, E., Li, H. wen, 2017. Hydrogen - A sustainable energy carrier. Prog. Nat. Sci. Mater. Int. 27, 34–40. https://doi.org/10.1016/j.pnsc.2016.12.014

Mouilleau, Y., Champassith, A., 2009. CFD simulations of atmospheric gas dispersion using the Fire Dynamics Simulator (FDS). J. Loss Prev. Process Ind. 22, 316–323. https://doi.org/10.1016/j.jlp.2008.11.009

Na'inna, A.M., Phylaktou, H.N., Andrews, G.E., 2013. The acceleration of flames in tube explosions with two obstacles as a function of the obstacle separation distance. J. Loss Prev. Process Ind. 26, 1597–1603. https://doi.org/10.1016/j.jlp.2013.08.003

Popat, N.R., Catlin, C.A., Arntzen, B.J., Lindstedt, R.P., Hjertager, B.H., Solberg, T., Saeter, O., Van Den Berg, A.C., 1996. Investigations to improve and assess the accuracy of computational fluid dynamic based explosion models. J. Hazard. Mater. 45, 1–25. https://doi.org/10.1016/0304-3894(95)00042-9

Puggelli, S., Veynante, D., Vicquelin, R., 2021. Impact of dynamic modelling of the flame subgrid scale wrinkling in large-Eddy simulation of light-round in an annular combustor. Combust. Flame 230. https://doi.org/10.1016/j.combustflame.2021.111416

Rochette, B., Collin-Bastiani, F., Gicquel, L., Vermorel, O., Veynante, D., Poinsot, T., 2018. Influence of chemical schemes, numerical method and dynamic turbulent combustion modeling on LES of premixed turbulent flames. Combust. Flame 191, 417–430. https://doi.org/10.1016/j.combustflame.2018.01.016

Schmitt, T., Boileau, M., Veynante, D., 2015. Flame Wrinkling Factor Dynamic Modeling for Large Eddy Simulations of Turbulent Premixed Combustion. Flow, Turbul. Combust. 94, 199–217. https://doi.org/10.1007/s10494-014-9574-0

Tong, H., Yao, Z., Lim, J.W., Mao, L., Zhang, J., Ge, T.S., Peng, Y.H., Wang, C.H., Tong, Y.W., 2018. Harvest green energy through energy recovery from waste: A technology review and an assessment of Singapore. Renew. Sustain. Energy Rev. 98, 163–178. https://doi.org/10.1016/j.rser.2018.09.009

Vermorel, O., Quillatre, P., Poinsot, T., 2017. LES of explosions in venting chamber: a test case for premixed turbulent combustion models. Combust. Flame 183, 207–223.

Versteeg, H.K., Malalasekera, W., 2007. An introduction to computational fluid dynamics - the finite volume method, Second Ed. ed. Pearson.

Veynante, D., Moureau, V., 2015. Analysis of dynamic models for large eddy simulations of turbulent premixed combustion. Combust. Flame 162, 4622–4642. https://doi.org/10.1016/j.combustflame.2015.09.020

Volpiani, P.S., Schmitt, T., Veynante, D., 2017. Large eddy simulation of a turbulent swirling premixed flame coupling the TFLES model with a dynamic wrinkling formulation. Combust. Flame 180, 124–135. https://doi.org/10.1016/j.combustflame.2017.02.028

Vyazmina, E., Jallais, S., 2016. Validation and recommendations for FLACS CFD and engineering approaches to model hydrogen vented explosions: effects of concentration, obstruction vent area and ignition position. Int. J. Hydrogen Energy 41, 15101–15109. https://doi.org/10.1016/j.ijhydene.2016.05.189

Wang, G., Boileau, M., Veynante, D., 2011. Implementation of a dynamic thickened flame model for large eddy simulations of turbulent premixed combustion. Combust. Flame 158, 219–213.

Wang, G., Boileau, M., Veynante, D., Truffin, K., 2012. Large eddy simulation of a growing turbulent premixed flame kernel using a dynamic flame surface density model. Combust. Flame 159, 2742–2754. https://doi.org/10.1016/j.combustflame.2012.02.018

Wen, X., Yu, M., Liu, Z., Sun, W., 2012. Large eddy simulation of methane–air deflagration in an obstructed chamber using different combustion models. J. Loss Prev. Process Ind. 25, 730–738. https://doi.org/10.1016/j.jlp.2012.04.008

Werner, H., Wengle, H., 1993. Large-Eddy Simulation of Turbulent Flow Over and Around a Cube in a Plate Channel, in: Durst, F., Friedrich, R., Launder, B.., Schmidt, F.., Schumann, U., Whitelaw, J.H. (Eds.), Turbulent Shear Flows 8. Springer, Berlin, Heidelberg.

Williamson, J., Mcgill, J., Trouve, A., 2005. Large Eddy Simulation Modeling Of Turbulent Deflagrations. Fire Saf. Sci. 8, 1375–1386.

https://doi.org/10.3801/IAFSS.FSS.8-1375